The Early Winter Sea Ice Variability under the Recent Arctic Climate Shift*

XIAO-YI YANG

State Key Laboratory of Marine Environmental Science, and College of Ocean and Earth Sciences, Xiamen University, Xiamen, China

XIAOJUN YUAN

Lamont-Doherty Earth Observatory, Columbia University, Palisades, New York

(Manuscript received 2 September 2013, in final form 14 February 2014)

ABSTRACT

This study reveals that sea ice in the Barents and Kara Seas plays a crucial role in establishing a new Arctic coupled climate system. The early winter sea ice before 1998 shows double dipole patterns over the Arctic peripheral seas. This pattern, referred to as the early winter quadrupole pattern, exhibits the anticlockwise sequential sea ice anomalies propagation from the Greenland Sea to the Barents–Kara Seas and to the Bering Sea from October to December. This early winter in-phase ice variability contrasts to the out-of-phase relationship in late winter. The mean temperature advection and stationary wave heat flux divergence associated with the atmospheric zonal wave-2 pattern are responsible for the early winter in-phase pattern.

Since the end of the last century, the early winter quadrupole pattern has broken down because of the rapid decline of sea ice extent in the Barents–Kara Seas. This remarkable ice retreat modifies the local ocean–atmosphere heat exchange, forcing an anomalous low air pressure over the Barents–Kara Seas. The subsequent collapse of the atmospheric zonal wave-2 pattern is likely responsible for the breakdown of the early winter sea ice quadrupole pattern after 1998. Therefore, the sea ice anomalies in the Barents–Kara Seas play a key role in establishing new atmosphere–sea ice coupled relationships in the warming Arctic.

1. Introduction

Recent Arctic climate differs greatly from that in the second half of the twentieth century. The Arctic Oscillation (AO), the primary mode of the extratropical atmospheric circulation, declines from a strong positive phase to an almost neutral state during the recent two decades (Cohen and Barlow 2005; Overland and Wang 2005), and its spatial structure shifts from the conventional tripolar to a dipolar pattern (Zhang et al. 2008). Because of the alleviation of AO-related atmospheric poleward energy transport, the pan-Arctic warming in the free troposphere/lower stratosphere layer has slowed down (Yang et al. 2010; Alexeev et al. 2012). The Arctic surface temperature, however, has soared in association with the abrupt acceleration of the Arctic sea ice thinning and retreat after 1990s (Serreze et al. 2007; Chapman and Walsh 2007; Overland et al. 2008; Nghiem et al. 2007; Maslanik et al. 2007). The long-term ocean observations also reveal the unprecedented warming of the intermediate Atlantic water in the Arctic Ocean since 2000 (Polyakov et al. 2012). In evaluating various factors responsible for the Arctic temperature amplification, Screen and Simmonds (2010) concluded that the diminishing Arctic sea ice has had a leading role in recent Arctic surface warming.

Many previous studies associated the thinning and retreat of Arctic sea ice to the atmospheric AO variability (Rigor et al. 2002; Zhang et al. 2003; Stroeve et al. 2007). In light of the recent decoupling of AO with the surface Arctic climate, Lindsay and Zhang (2005) proposed that the Arctic climate has entered a new climate regime thermally driven by the effect of an ice–albedo feedback. This effect is primarily felt in late autumn and early winter, when the ocean loses the extra heat gained during summer to facilitate the sea ice growth (Serreze

*Lamont-Doherty Earth Observatory Publication Number 7787 and Xiamen University Publication Number 2014018.

Corresponding author address: Xiao-Yi Yang, C3-418, Xiping Building, Xiang An Campus, Xiamen University, Xiang An Nan Road, Xiamen, Fujian 361102, China.
E-mail: xyyang@xmu.edu.cn

DOI: 10.1175/JCLI-D-13-00536.1

© 2014 American Meteorological Society

and Barry 2011). Hence, the Arctic sea ice extent in this transition season is preconditioned by the extent of summer ice retreat. On the other hand, the extending sea ice cover insulates the turbulent heat flux from ocean and thermally feedbacks to the overlying atmosphere. Some recent studies explored the possibility of September sea ice minima influencing the atmospheric circulation in the following autumn and winter (Francis et al. 2009; Strey et al. 2010; Hopsch et al. 2012; Orsolini et al. 2012). Among others, Deser et al. (2010) have noted the baroclinic feature of atmospheric response to the Arctic sea ice losses in early winter (November–December), which contrasts to the barotropic responses in late winter (January–March). Screen et al. (2013) further declared that the atmospheric response to the sea ice loss is most pronounced in autumn and early winter, and the resulting earlier onset of baroclinic instability can impact the structure of large-scale planetary waves in late winter (Jaiser et al. 2012). It seems that the sea ice variability in early winter and its interaction with the atmospheric circulation may be a key factor to understand the recent Arctic climate shift.

At time scales from weeks to decades, winter arctic sea ice variability is dominated by two sets of dipole pattern in the Arctic marginal seas, with the out-of-phase variations of sea ice concentration (SIC) between the Bering Sea (Ber) and the Okhotsk Sea (Okh) in the Pacific sector and between the Baffin–Labrador Seas (BaL) and the Greenland–Barents–Kara Seas in the Atlantic sector (Fang and Wallace 1994; Deser et al. 2000). Proshutinsky and Johnson (1997) suggested that the winter Arctic sea ice variability is forced by changes in the location and intensity of the Icelandic low (IL) and the Siberian high. The study by Francis and Hunter (2007) revealed that the Bering Sea ice variability is influenced mainly by anomalies in easterly winds associated with the Aleutian low (AL), whereas the Barents Sea ice is driven primarily by sea surface temperature and the local meridional wind. So far, we do not know whether this quadrupole pattern of winter sea ice variability remains robust under the new Arctic climate regime. Less known is the sea ice variability in the late autumn/early winter season, when the Arctic sea ice cover extends from the Arctic Ocean to the marginal seas and the atmospheric semipermanent active centers (i.e., AL and IL) are not steadily established.

This study aims to investigate the interannual variability of sea ice concentration in late autumn/early winter (October–December) in the context of the climate regime shift during the late 1990s. Here we identify a connection between the sea ice anomalies in the marginal seas of the Atlantic sector of the Arctic [including the Greenland Sea (Grn) and the Barents–Kara Seas (BaK)] and in the Ber during October through December, which is different from the quadrupole teleconnection pattern found in late winter. We then investigate mechanisms that lead to this early winter covariability in sea ice across the Arctic Basin. Furthermore, we find that this early winter sea ice teleconnection breaks down after the late 1990s, when the BaK ice variability is thermally driven by ice–albedo feedback and the Grn ice variability is mostly controlled by the atmospheric circulation. This will in turn block the energy propagation of planetary wave from the North Atlantic to the North Pacific and weaken the teleconnection of sea ice variability across the Arctic.

The paper is composed of six sections. Section 2 introduces the data and method. The contrast in spatial patterns of SIC and sea ice extent (SIE) between the periods of 1979–97 and 1998–2012 is explored in section 3. Section 4 investigates the underlying mechanisms that lead to the sea ice covariability in early winter. The mechanism that may responsible to the breakdown of the sea ice covariability in the recent warming climate regime is studied in section 5. Discussion and conclusions are presented in the last section.

2. Data and method

The monthly data of SIC and sea surface temperature (SST) are obtained from the Met Office Hadley Centre Sea Ice and Sea Surface Temperature dataset version 1 (HadISST1) (Rayner et al. 2003). The data resolution is $1° \times 1°$ with the period ranging from January 1979 to December 2012. The period is chosen for the reason that the satellite SIC data are continuously available since October 1978 and the HadISST SIE data before 1979 are likely overestimated, according to Stroeve et al. (2012). The SIE time series was generated by summing the areas of all grid boxes with at least 15% ice concentration. In addition, the SIE time series from the National Snow and Ice Data Center (NSIDC) was applied to verify the results of HadISST1. The time series was calculated from SIC derived by the National Aeronautics and Space Administration (NASA) team algorithm from *Nimbus-7* Scanning Multichannel Microwave Radiometer (SMMR; 1978–87), Defense Meteorological Satellite Program (DMSP) Special Sensor Microwave Imager (SSM/I; 1987–2009), and DMSP Special Sensor Microwave Imager/Sounder (SSM/IS; 2008–10) satellite passive microwave radiances on a 25 km $\times$ 25 km polar stereographic grid (Cavalieri et al. 2013). Figure 1a shows the time series of the total Arctic sea ice extent in September. Compared to NSIDC satellite data, the HadISST data may underestimate the sea ice decline after the late 1990s. Nevertheless, a high consistency can

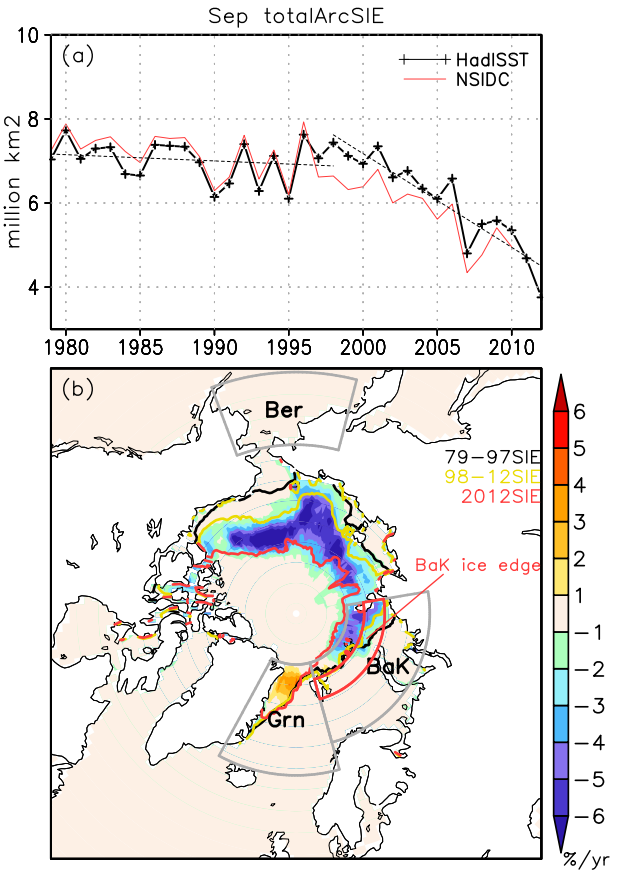

FIG. 1. (a) Total September Arctic sea ice extent (SIC ≥ 15%) during 1979–2012 from HadISST (black) and NSIDC datasets (red), superimposed with the linear trends of the early period (1979–98) and the late period (1998–2012) (black dashed) (units: millions of square kilometers). (b) Linear trends grid by grid during the late period (shaded area; unit: % yr^{-1}), with the solid lines indicating the climatological September sea ice edges for the early period (black), the late period (yellow), and the sea ice edge in September 2012. The three Arctic peripheral seas (Grn, BaK, and Ber) are defined by gray boxes, and the red box indicates the BaK ice edge zone.

be readily seen in these two observational time series with the year-to-year correlation of 0.91 for the period from 1979 to 2010. The trends based on the HadISST dataset are quite consistent with the satellite data; hence, the results are not sensitive to the dataset chosen.

The monthly-mean atmospheric data used here are from the National Centers for Environmental Prediction–National Centers for Atmospheric Research (NCEP–NCAR) reanalysis dataset with a horizontal resolution of 2.5° × 2.5°, with 17 vertical levels from 1000 to 10 hPa (Kalnay et al. 1996). Physical variables used in this study include sea level pressure, air temperature, zonal and meridional winds, and geopotential heights. Daily data of temperature and zonal and meridional winds are also applied to calculate the transient heat flux. We have verified that the results of this study are robust regardless which reanalysis dataset is chosen.

To diagnose the three-dimensional propagation of stationary waves in association with the sea ice extent anomalies in the North Atlantic the generalized stationary wave activity flux (F_s) is derived by following Plumb (1985),

$$F_s = p\cos\phi \times \left\{ \begin{array}{l} v'^2 - \dfrac{1}{2\Omega a \sin 2\phi}\dfrac{\partial(v'\Phi')}{\partial\lambda} \\ -u'v' + \dfrac{1}{2\Omega a \sin 2\phi}\dfrac{\partial(u'\Phi')}{\partial\lambda} \\ \dfrac{2\Omega\sin\phi}{S}\left[v'T' - \dfrac{1}{2\Omega a \sin 2\phi}\dfrac{\partial(T'\Phi')}{\partial\lambda}\right] \end{array} \right\}.$$

Here, the terms u, v, Φ, ϕ, and T are the horizontal winds, geopotential, latitude, and air temperature, respectively. The prime denotes the variable deviation from the zonal mean at each latitude and height. The term S is the static stability, defined as $S = (\partial\hat{T}/\partial z) + (\kappa\hat{T}/H)$, with the caret indicating an area average in the extratropical Northern Hemisphere; H is the scale height $H = -(\hat{z}/\ln p)$, and κ is the constant, expressed as $\kappa = R/C_p \approx 0.286$.

3. Contrast of the early winter Arctic sea ice variability before and after 1998

Model and observational data analysis reveal that memory of the Arctic sea ice anomalies can persist at least 2 months (Blanchard-Wrigglesworth et al. 2011). While the September Arctic sea ice cover experiences the dramatic retreat during the last three decades, it is expected to impact the sea ice growth in the following October and November by changing the upper-ocean heat content. Figure 1a clearly shows that the decline of the sea ice extent has accelerated in the recent decade. The sea ice extent trends are $-0.14 \times 10^6\,km^2$ (−2.1%) per decade for the period of 1979–98 and $-2.08 \times 10^6\,km^2$ (−31.6%) per decade for the period of 1998–2012. The trend estimate for the early period is not sensitive to the start and end points and is largely consistent with the satellite data results (Comiso et al. 2008). However, the trend estimate for the late period is larger than the 1997–2007 trend calculated by Comiso et al. (2008), which is due to the abrupt sea ice decline in the recent 2 yr. In fact, the September 2012 sea ice cover becomes the new record minimum (less than $4 \times 10^6\,km^2$) (Parkinson and Comiso 2013; Holland 2013); if the year 2012 is subtracted from the late period, the trend slope is reduced to $-1.84 \times 10^6\,km^2$ (−27.9%) per decade. The linear trends of September SIC during

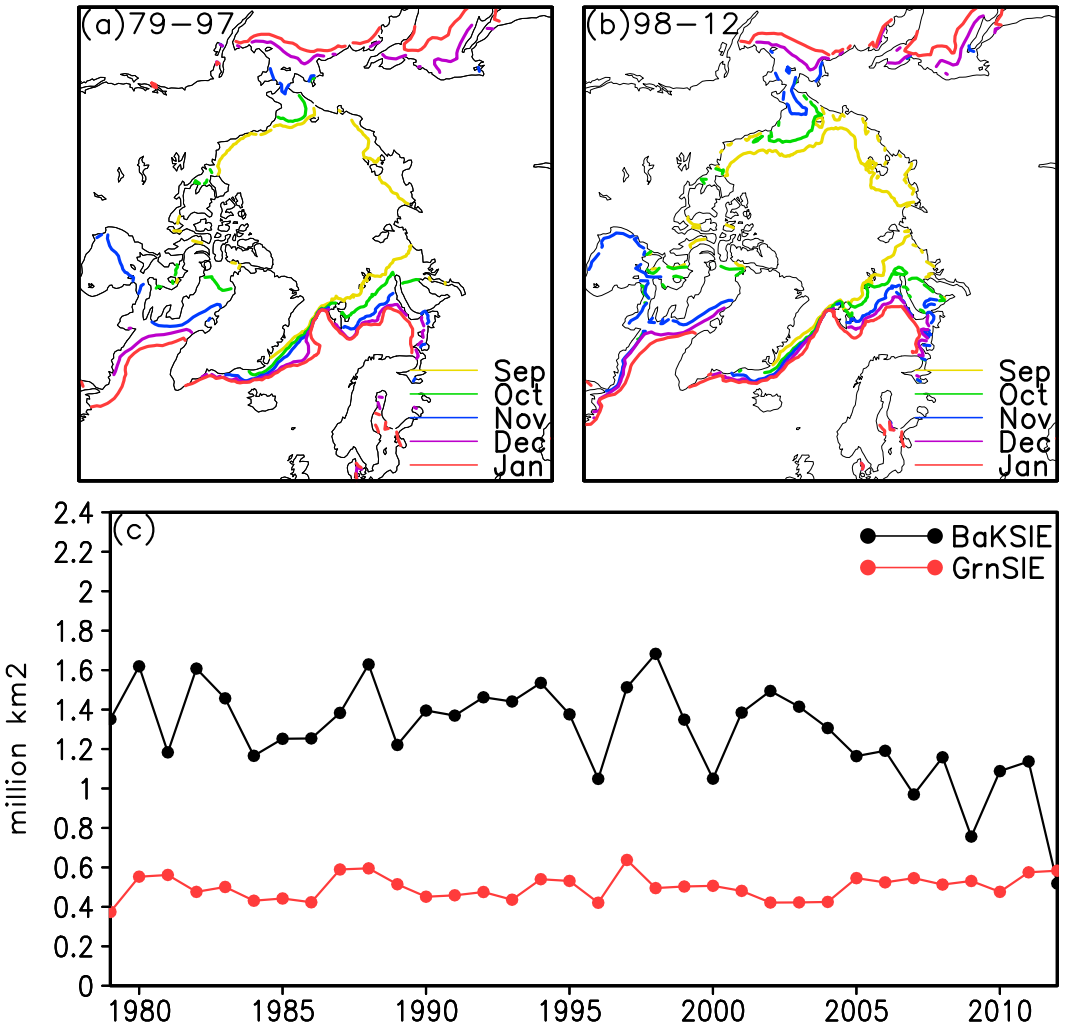

FIG. 2. (a) Monthly (September–January) climatology of sea ice edge (SIC ≥ 15%) advance during the period of 1979–97. (b) As in (a), but for the period of 1998–2012. (c) Time series of November Barents–Kara Seas ice extent (black lines) and November Greenland sea ice extent (red lines) (unit: millions of square kilometers).

1998–2012 are plotted at grid points in Fig. 1b, superimposed by the September climatological sea ice edge (SIC ≥ 15%) during the periods of 1979–97 (the early period) and 1998–2012 (the late period) and the ice edge in September 2012. Also marked by the gray lines are the areas of the three Arctic peripheral seas: the Greenland Sea, the Barents–Kara Seas, and the Bering Sea. The remarkable retreat of perennial sea ice occurs in the eastern Arctic Ocean including the Beaufort Sea, the East Siberian Sea, the Laptev Sea, and the BaK. The western Arctic experiences no significant SIC reduction or sea ice edge retreat. Even a moderate positive trend of SIC appears in the Grn, which may be attributed to the excessive multiyear sea ice export through the Fram Strait by the transpolar drift stream.

The seasonal migration of the sea ice edge from September to January are shown in Figs. 2a,b for the early and late periods, respectively. The sea ice cover extends from the Arctic Ocean to the peripheral seas in early winter, first to the North Atlantic in October–November and then to the North Pacific in December. Among all the peripheral seas, the most drastic extension of sea ice edges occurs in the BaK. Francis and Hunter (2007) found that the hemispheric-mean decline in winter SIE is due in large part to increasing SST in the Barents Sea and adjacent waters. It is reasonable that the November BaK sea ice bears the signal of the pan-Arctic sea ice retreat in September and hence exhibits a significant downward trend after 1998 (Fig. 2c). On the contrary, the November Grn SIE shows no significant trend during the

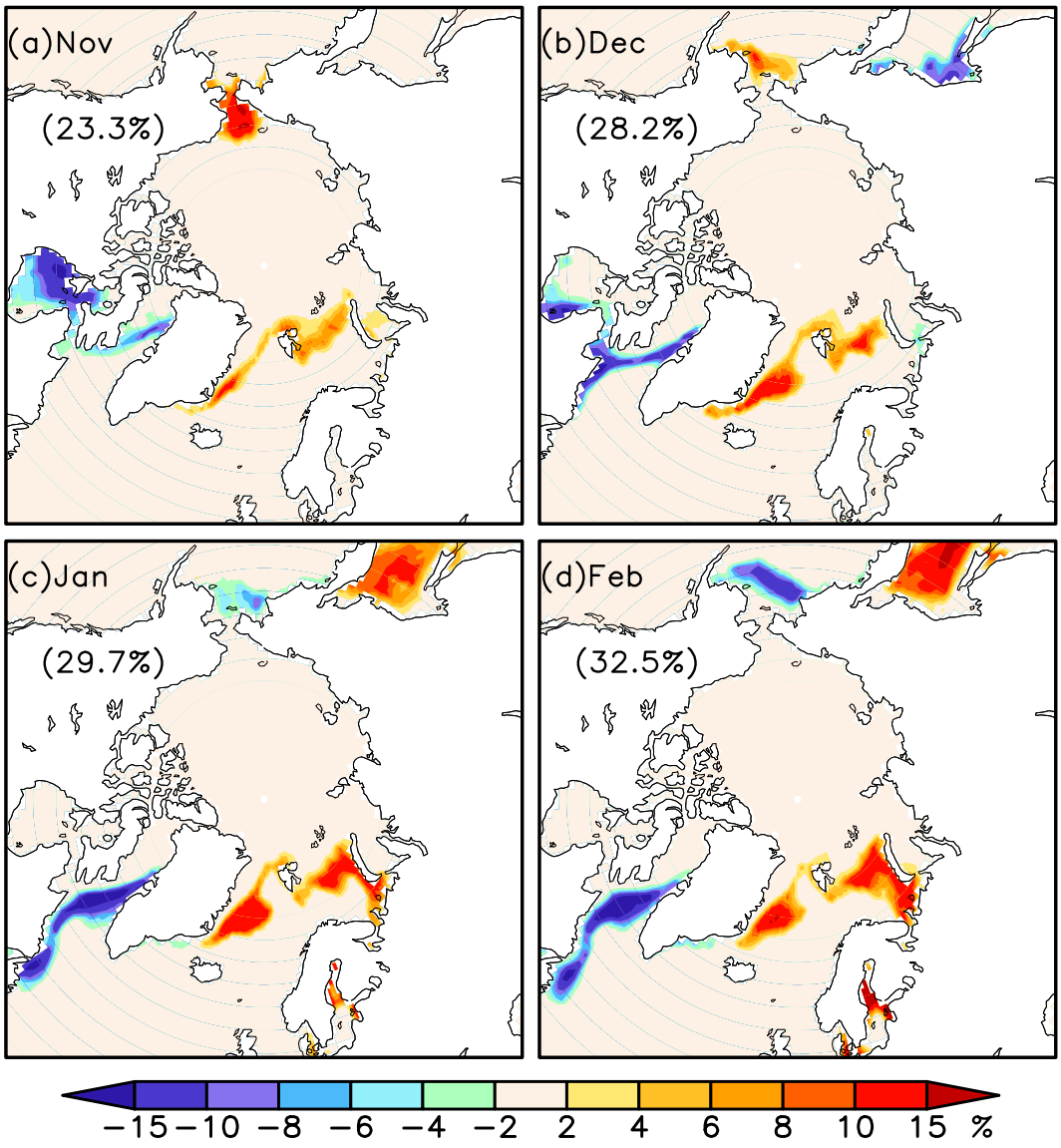

FIG. 3. Leading EOF modes of sea ice concentration in (a) November, (b) December, (c) January, and (d) February during the period of 1979–97. The total variances explained by the leading modes are marked in the panels, which are all well separated from the second modes.

whole period, consistent with the September SIC trends in Fig. 1b.

To investigate covariability of sea ice in the Arctic and its peripheral marginal seas, the analysis of empirical orthogonal function (EOF) is applied to the SIC anomalies in the wintertime. The leading EOF modes of SIC in each month from November to February of 1979–97 are presented in Fig. 3, which are well separated from the second modes and explain 23.3%, 28.2%, 29.7%, and 32.5%, respectively, of the total variance of each month. Throughout the whole wintertime, the SIC variability exhibits two dipole patterns: there are out-of-phase ice anomalies in the Grn–BaK and the BaL in the North Atlantic and out-of-phase ice anomalies in the Ber and the Okh in the North Pacific. An ice tongue appears in the Grn from December to February, which is referred as the winter Odden ice feature in previous studies (Deser et al. 2000). The Odden is a tongue of sea ice that episodically advances rapidly northeastward into the Grn from the edge of the main ice pack near 10°W between 72° and 74°N (Shuchman et al. 1998). This phenomenon, according to Rogers and Hung (2008), may be closely related to the anomalous westerly wind associated with the North Atlantic Oscillation (NAO). Nevertheless, the sea ice variability in early winter is apparently contrasted to that in late winter. The

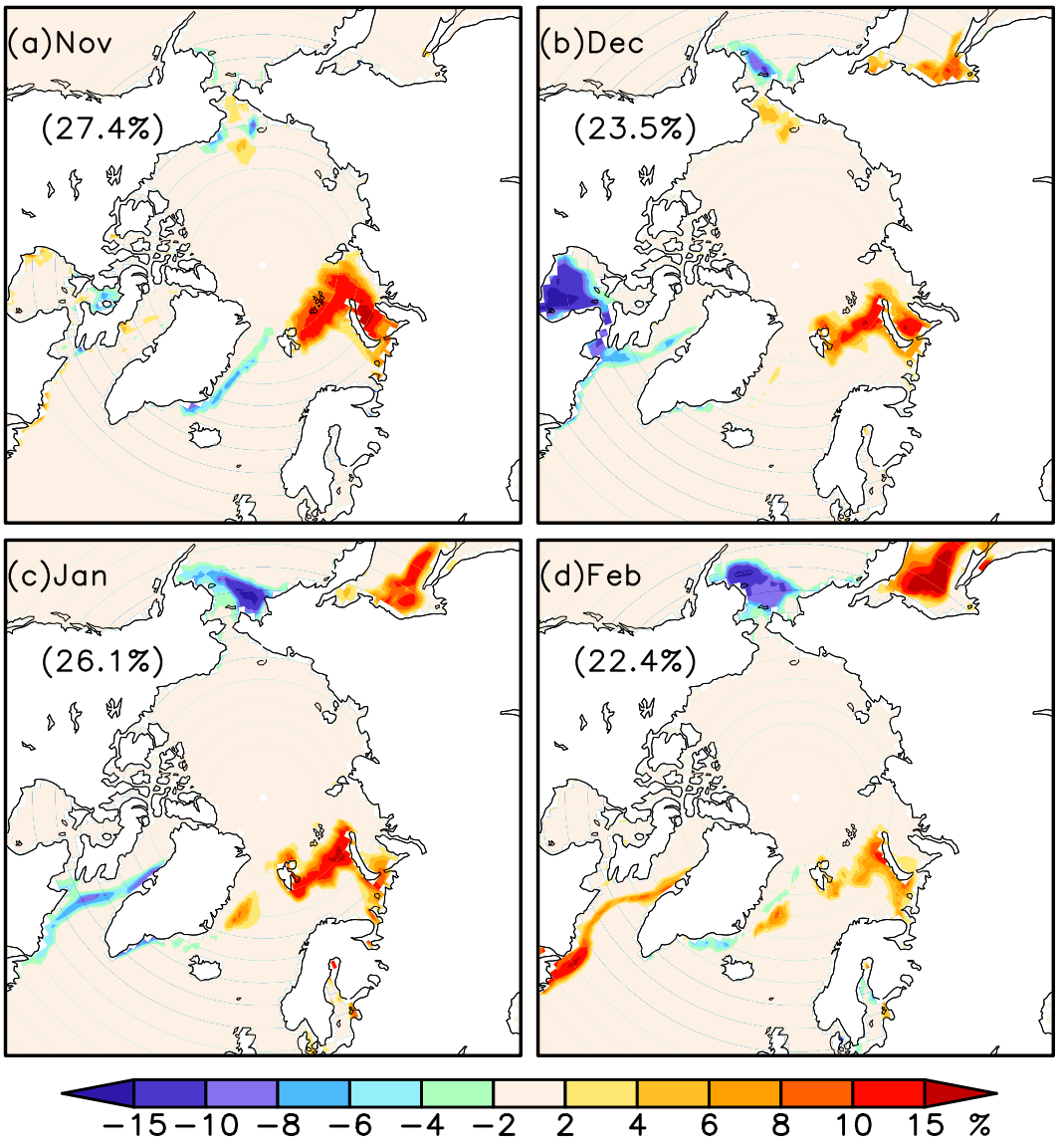

FIG. 4. As in Fig. 3, but for the period of 1998–2012.

hemispheric-scale SIC variability exhibits a longitudinal anticlockwise +/−/+/− pattern from Grn–BaK to BaL in early winter (Figs. 3a,b), while in late winter it turns to be a +/+/−/− pattern (Figs. 3c,d). In other words, the Ber SIC varies in phase with the Grn–BaK SIC in early winter and reverses to out of phase in late winter. We call the +/−/+/− pattern as the early winter quadrupole pattern.

Consistent with the asymmetric SIE trends after 1998 (Fig. 2c), the November SIC leading EOF mode is predominated by the BaK SIC anomalies in the late period (Fig. 4a) and its time series shows a significant downward trend (not shown). The late winter quadrupole pattern reappears in December–January (Figs. 4b,c), but the leading modes account for less variance compared to those in the early period. In February (Fig. 4d), sea ice variance is mostly confined in the North Pacific as a seesaw pattern between Ber and Okh while the anomalies in the North Atlantic are much weaker. The EOF1 time series also presents a strong downward trend (not shown). This result is qualitatively consistent with the study by Parkinson and Cavalieri (2008). The most notable change in the late period is the breakdown of the early winter quadrupole pattern. The Grn SIC anomalies become much weaker and independent from the BaK SIC anomalies. The winter Odden feature in the Grn almost disappears after 1998, which is likely attributed to the weakening of the westerly wind in

association with the polarity shift of AO/NAO mode. Particularly in November, Grn SIC seems to be out of phase with the BaK SIC anomalies, whereas they are largely in phase in the early period.

The robustness of phase relationships in SIC anomalies revealed by the leading EOF modes can be verified by the lead–lag correlations among the detrended Ber SIE, Grn SIE, and BaK SIE (Fig. 5). For the early period, the positive correlations between the BaK SIE and Grn SIE prevail from early winter throughout late winter, with the maximum over 0.7 in January and February (Fig. 5a). Significant positive correlations also arise between the Ber SIE and Grn (BaK) SIE in early winter, which turns into negative correlations in late winter (Figs. 5b,c). This corresponds to the quadrupole pattern shift from early winter to late winter (Fig. 3). We notice that the correlation among these three seas is not simultaneous, because the maximum correlations deviate from the zero-lag line. Instead, the sea ice variability seems to be in an anticlockwise sequence that the October Grn SIE anomalies are followed by November BaK SIE anomalies and then the Ber SIE anomalies in December and January. This anticlockwise relationship fades away during the late period (Figs. 5d–f). The November Grn SIE anomalies negatively (positively) correlate with the December–January BaK SIE (Ber SIE) but with no significant correlations between the BaK SIE and Ber SIE. Neither has a significant correlation in late winter. Similar results have been reproduced in NSIDC satellite data and in the original HadISST SIE data with the trends included.

4. The mechanisms for the early winter sea ice teleconnection

Deser et al. (2000) explicitly stated that winter SIC anomalies are directly forced by the atmosphere, either thermodynamically through temperature advection or dynamically through wind-driven ice drift. Winter atmospheric circulation is dominated by the AL over the North Pacific and IL over the North Atlantic. It is sensible that the out-of-phase relationship between the Ber SIE and the Grn–BaK SIE (Figs. 5b,c) is caused by the AL–IL seesaw pattern in late winter (Honda et al. 2001; Honda et al. 2005b). However, what fuels the covariability of sea ice cover with the early winter quadrupole pattern? Why do the ice anomalies in the North Pacific appear 1–2 months later than those in the North Atlantic? To understand this phenomenon, we first investigate the anomalous atmospheric circulation associated with November sea ice anomalies in the Atlantic sector of the Arctic and examine its evolution from October to December.

We plot the detrended and normalized November Grn SIE and BaK SIE time series in Fig. 6. The relationship between these two time series changes remarkably before and after 1998, with the correlation coefficients of 0.48, −0.61, and almost zero for the periods of 1979–97, 1998–2012, and 1979–2012, respectively. The years with the collaborative advance (retreat) of the November Grn SIE and the BaK SIE (exceeding ±0.5 standard deviation) in the early period (Table 1, columns 1 and 2) are selected to do the composite analysis. The composites of early winter (October–December) sea level pressure (SLP) and 850-hPa horizontal winds are presented in Fig. 7 (left). In October, the anomalous atmospheric circulation is basically an Arctic dipole pattern with the high pressure residing over the Greenland and Iceland region and the low pressure residing over the East Siberian Sea (Fig. 7a). This dipole pattern is quite similar to that described by Wu et al. (2006), who asserted that the large-scale changes in the intensity of sea ice transport are associated with this mode, leading to positive ice cover anomalies in the Grn–BaK region. In addition, the SLP dipole mode is accompanied by an anomalous strong transpolar wind from the Chukchi Sea through the Greenland Sea and the Norwegian Sea. Aside from the dynamical effect, these northerly winds generate the cold advection bringing polar air to the Grn, thermodynamically preconditioning the region for sea ice growth. In November, the high pressure migrates eastward to the east of Iceland. A wave-2 SLP pattern, with lows over North America and Northern Europe and highs near Iceland and the Aleutian Basin, emerges in the subpolar regions (Fig. 7d). Accordingly, the northerly winds at the east flank of the anomalous highs prevail over both the BaK and the Ber and then facilitate the local sea ice increase. In December, an anomalous low pressure and the associated cyclonic winds appear over the Arctic Ocean (Fig. 7g). The anomalous meridional winds become much weaker in the Atlantic, but the northerly winds associated with the high anomalies continue to predominate over the Ber. It seems that the sea ice anomalies keep the pace of the anomalous northerly winds, which prevail in the Grn, BaK, and Ber successively from October to December. Thus, the Grn–BaK SIC-related large-scale atmospheric circulation may contribute to the in-phase relation between the Grn SIC, BaK SIC, and Ber SIC, leading to the early winter quadrupole pattern.

To further examine the role of Grn–BaK SIC in the early winter sea ice–atmosphere interaction process, we regress SLP anomalies (in October, November, and December) on the principle component of the leading EOF mode of November SIC anomalies (Figs. 7b,e,h).

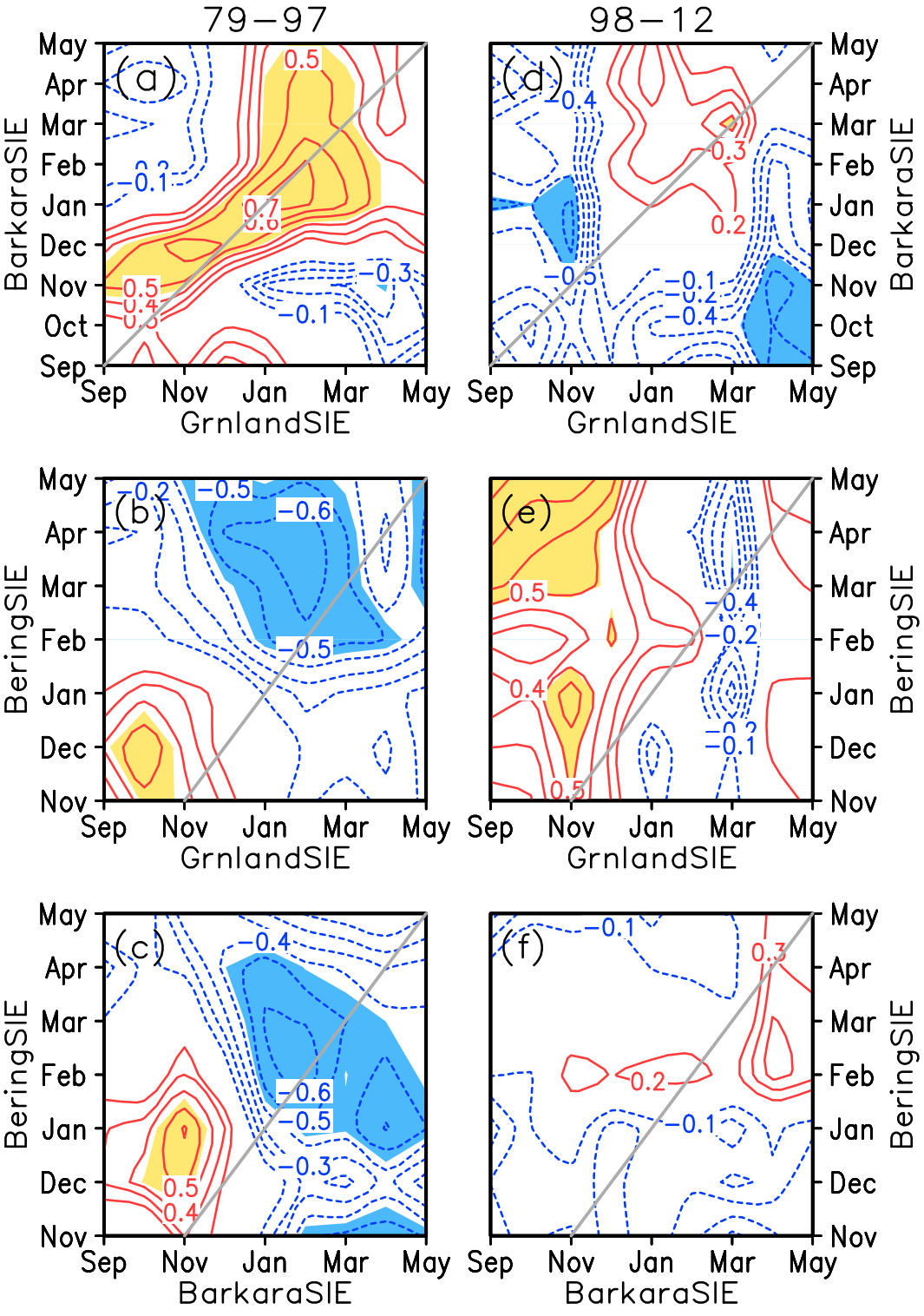

FIG. 5. (a) Detrended lead–lag correlations between the Barents–Kara Sea ice extent and the Greenland Sea ice extent during the period of 1979–97. The contour interval is 0.1, and the shaded area denotes the correlation coefficients above the 95% significance level of Student's *t* test. The gray line marks the zero-lag correlations. (b) As in (a), but for sea ice extent between the Greenland Sea and the Bering Sea. (c) As in (a), but for sea ice extent between the Barents–Kara Seas and the Bering Sea. (d)–(f) As in (a)–(c), but for the period of 1998–2012.

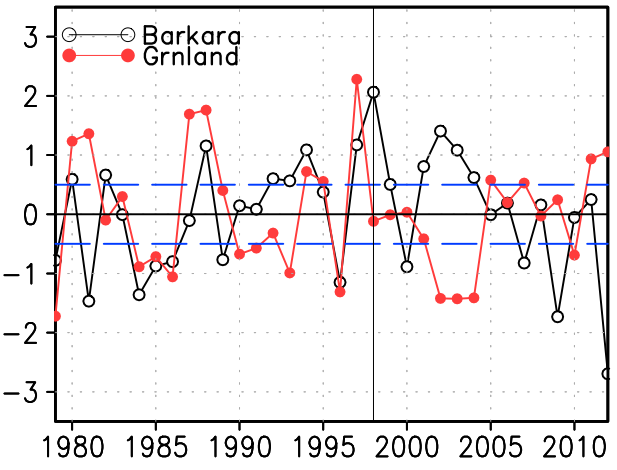

FIG. 6. Normalized and detrended November sea ice extent indices of the Barents–Kara Seas (black) and the Greenland Sea (red) during the period of 1979–2012. The gray line indicates the year 1998, and the blue dashed lines denote the ±0.5 standard deviations.

Also shown in Fig. 7 are the leading modes of SLP EOF for the early periods (right panels). In October, the anomalous high pressure over the Iceland is mostly reproduced in both the regression pattern and the SLP EOF leading mode. It is clear that the weakening of atmospheric IL preconditions the synchronous advance of sea ice in the Grn–BaK. The Arctic dipole mode, though not as significant as in the composites, also exists in the regressions and EOF1 mode (Figs. 7a–c). More important, the early winter Grn–BaK SIC anomalies are highly coupled with the dominant atmospheric circulation, since the zonal wave-2 patterns in the composites, in the regressions, and in the EOF1 mode are extremely similar in November (Figs. 7d–f). In this sense, the atmospheric planetary wave is probably a key factor to the formation of early winter quadrupole pattern. The SIC-related atmosphere circulation in December shows an anomalous low and cyclonic winds over the Arctic and an anomalous high over the subpolar region (Figs. 7g,h). This pattern is similar to the winter atmospheric AO mode (Fig. 7i), again revealing that sea ice anomalies are associated with the dominant atmospheric pattern and play an important role in the coupled climate system.

Given the intense sea ice–atmosphere coupling in November, we investigate the dominant atmospheric circulation in November associated with Grn–BaK SIE anomalies. Figure 8 shows the composites in 250- and 500-hPa geopotential height, 850-hPa air temperature, and sea surface temperature anomalies associated with the November sea ice cover in the Grn–BaK. The planetary wave-2 pattern in the subpolar region correspondingly appears in 500- and 250-hPa height fields, suggesting a quasi-barotropic nature of the atmosphere. The anomalous low-level temperature field displays a quarter of phase shift from geopotential height anomalies in the North Atlantic, which to some extent signifies the baroclinic response of the atmosphere to the surface heating. The large-scale cold (warm) anomalies over the Grn–BaK (BaL) in the North Atlantic and over the Ber (Okh) in the North Pacific in Fig. 8c give rise to the anomalous cold (warm) SST in these regions through the air–sea turbulent heat flux, leading to the associated SIC quadrupole pattern and the in-phase variability of the Grn SIE, BaK SIE, and Ber SIE in early winter.

We further examine the cause of successive sequence of the sea ice anomalies from the Atlantic sector to the Pacific sector of the Arctic. The generalized Eliassen–Palm (EP) flux is a useful tool to diagnose the stationary wave energy propagation (Plumb 1985). In accordance with the increase (decrease) of November sea ice cover in the Grn–BaK, the 250-hPa wave activity fluxes manifest unanimous northeastward (southwestward) propagation in this region, with a significant eastward propagation over the Greenland Sea and a significant northward propagation over the Barents Sea (Fig. 9). This anomalous wave energy propagation may help to stimulate the planetary wave in the downstream region and then establish the zonal wave-2 pattern. At the same time, the vertical component of EP flux analogously differs between the high and the low sea ice conditions. For the latitude of 70°N, the most conspicuous difference is located in the lower troposphere of the Grn–BaK region (40°W–90°E), with the anomalous upward wave perturbation corresponding to the advance of the sea ice cover (Fig. 10). This result is qualitatively insensitive to the latitudes chosen. The fact that the upward wave perturbation originates from the boundary layer may to some extent be interpreted as the excessive turbulent

TABLE 1. Selected years with the standard deviation of above (below) 0.5 (−0.5), for the simultaneously advancing (retreating) November sea ice cover of Greenland–Barents–Kara Seas, as well as the November Greenland sea ice cover advancing (retreating) and Barents–Kara sea ice cover retreating (advancing).

	GrnSIE+BaKSIE+	GrnSIE−BaKSIE−	GrnSIE+BaKSIE−	GrnSIE−BaKSIE+
Early period (1979–97)	1980, 1988, 1994, 1997	1979, 1984, 1985, 1986, 1996	1981	1993
Late period (1998–2012)			2007, 2012	2002, 2003, 2004

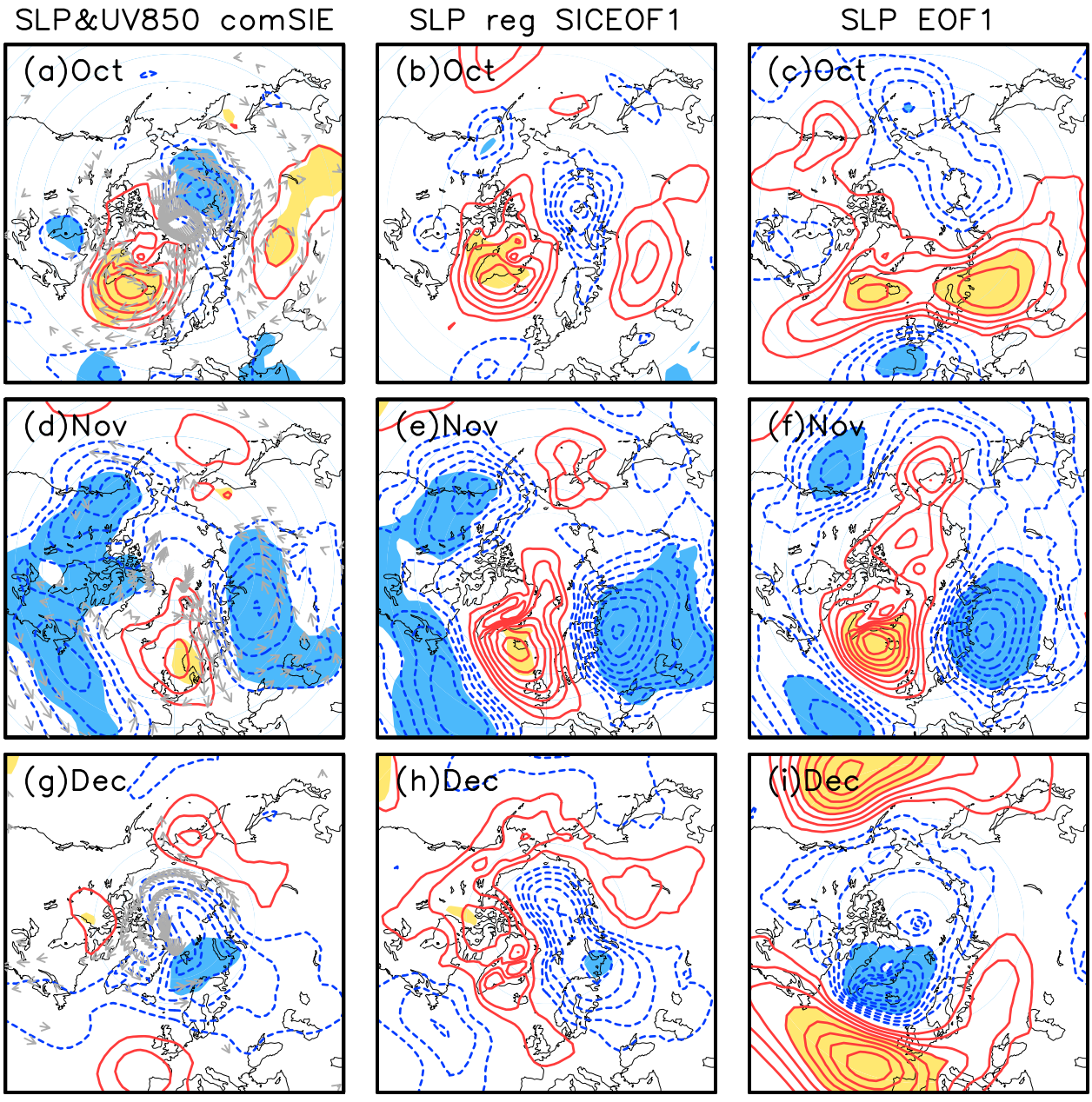

FIG. 7. (a) Detrended October sea level pressure anomalies (contours) and 850-hPa horizontal winds anomalies (vectors) composites based on the November Greenland–Barents–Kara sea ice extent indices in Fig. 6 (high minus low; for details, see Table 1). Contour intervals are 2 hPa with the 95% significance level signified by the shaded area. Only the zonal or the meridional winds above the 95% significance level are drawn as vectors. (b) Regression of 1979–97 detrended October sea level pressure anomalies on the time series of the leading EOF mode of November sea ice concentration. Contour intervals are 0.5 hPa, with the 95% significance level signified by the shaded area. (c) The leading mode of October detrended sea level pressure for the period of 1979–97, with contour intervals of 0.5 hPa and the shaded area denoting the anomalies above (below) 2 hPa (−2 hPa). (d)–(f) As in (a)–(c), but for the month of November. (g)–(i) As in (a)–(c), but for the month of December.

heat loss from the ocean due to the overlying cold air temperature (figure not shown). As the upward wave energy propagation is relevant to the northward eddy heat flux, it should in turn contribute to the low-level air temperature change.

To assess the contributions of various atmospheric internal processes to the 850-hPa temperature anomalies in early winter, we repeat the composite analysis for the mean temperature advection $-\overline{u}(\partial\overline{T}/\partial x) - \overline{v}(\partial\overline{T}/\partial y)$ (Fig. 11, left), the stationary wave heat flux convergence

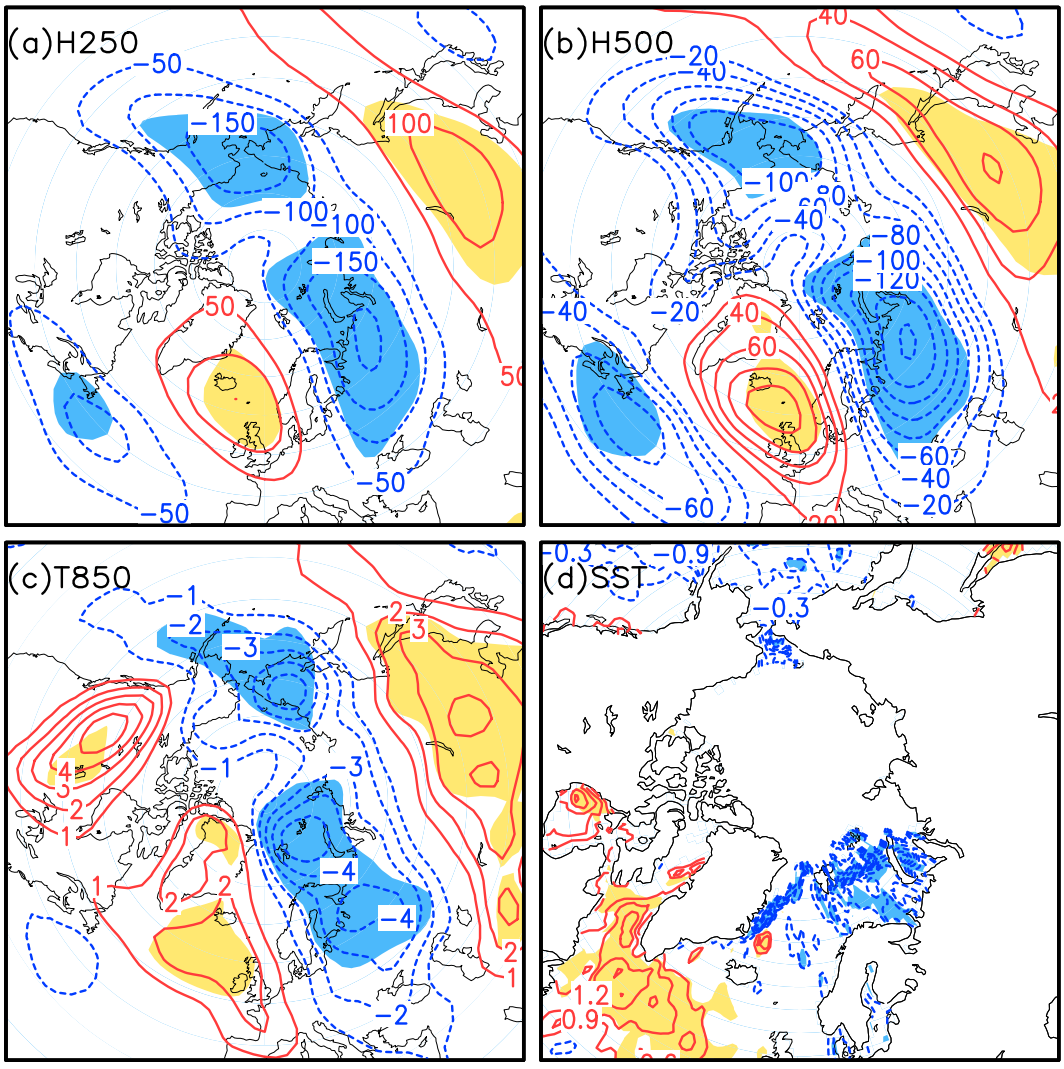

FIG. 8. (a) Detrended 250-hPa geopotential height composites based on the November Greenland–Barents–Kara sea ice extent indices in Fig. 6 (high minus low) [contour intervals: 50 geopotential meters (gpm); shaded area denotes the 95% significance level]. (b) As in (a), but for 500-hPa geopotential height (contour intervals: 20 gpm). (c) As in (a), but for 850-hPa air temperature (contour intervals: 1 K). (d) As in (a), but for sea surface temperature (contour intervals: 0.3 K).

$-[\partial(\overline{u}^*\overline{T}^*)/\partial x] - [\partial(\overline{v}^*\overline{T}^*)/\partial y]$ (Fig. 11, middle), and the transient wave heat flux convergence $-[\partial(\overline{u'T'})/\partial x] - [\partial(\overline{v'T'})/\partial y]$ (Fig. 11, right) based on the Grn SIE and BaK SIE indices shown in Fig. 6. The superscript primes and stars refer to the deviation from the monthly and zonal averages, respectively, while the overbars denote the monthly mean. The positive (negative) values indicate the warming (cooling) tendency in the units of Kelvins per day. In October–November, during the high sea ice years, the anomalous cold advection (Figs. 11a,d) and stationary wave heat flux divergence (Figs. 11b,e) prevail over the Grn–BaK region with almost equivalent magnitudes. The similar anomalous advection and heat flux divergence by stationary waves also predominate over the Bering Sea in November (Figs. 11d,e), persisting to December (Figs. 11g,h). Both the temperature advection and stationary wave heat flux divergence lead to the anomalous cold condition over the two regions in early winter, and their intraseasonal time evolution from the Grn (October) to the BaK (November) and then to the Ber (December) could well account for the phenomenon of the anticlockwise sequence of the sea ice anomalies. The heat flux from transient eddies, on the other hand, is less significant and acts to counteract the effect of the advection and stationary wave flux (Figs. 11c,f,i).

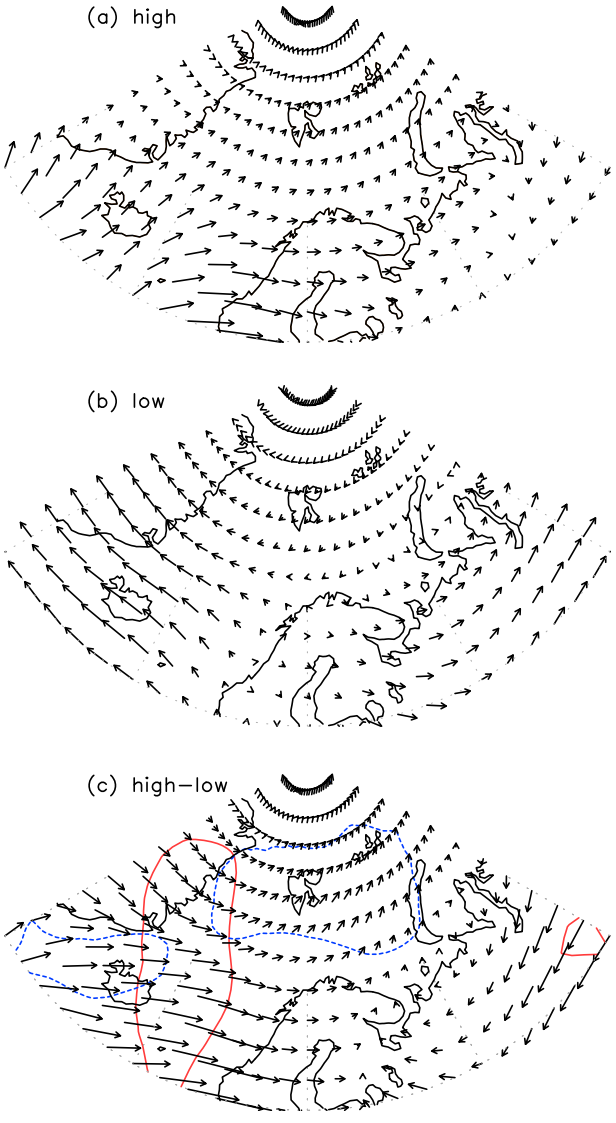

FIG. 9. (a) Detrended 250-hPa horizontal stationary wave activity flux over the North Atlantic region composites of the November Greenland–Barents–Kara sea ice extent high index events. (b) As in (a), but for low indices. (c) As in (a), but for high minus low indices. The contours denote the 95% significance level for zonal components of wave activity flux (red solid) and meridional components of wave activity flux (blue dashed).

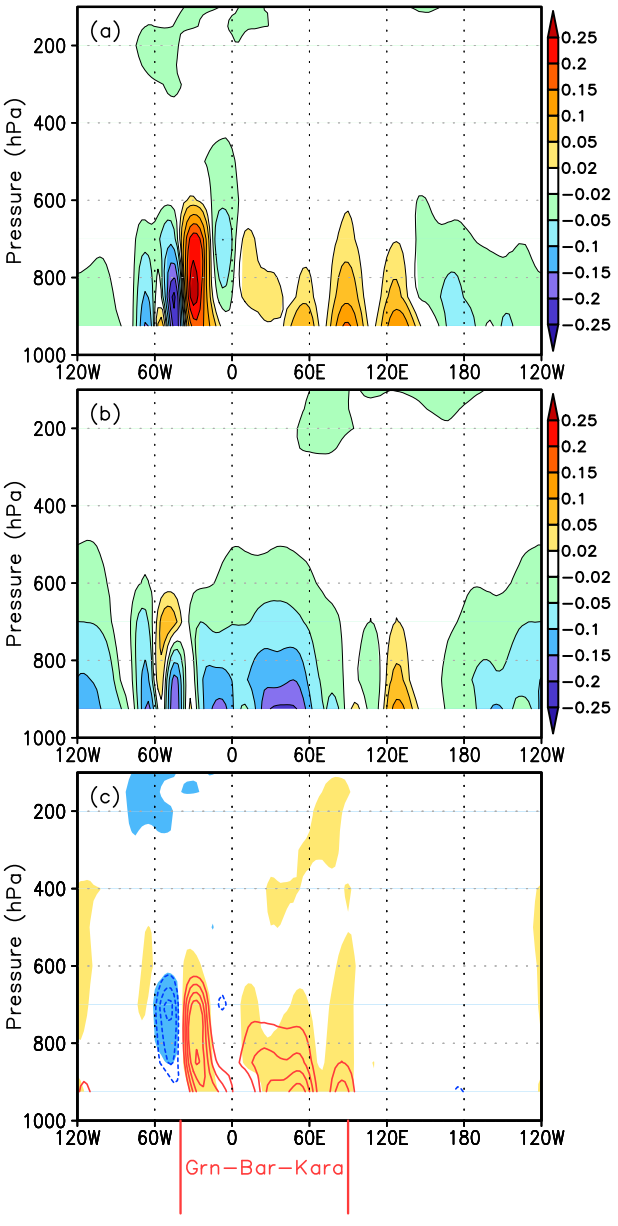

FIG. 10. As in Fig. 9, but for vertical stationary wave activity flux along the latitude of 70°N. Contour interval in (c) is 0.05 $m^2 s^{-2}$, and the shaded areas denote the 95% significance level. The two red lines mark the longitude positions of the Greenland–Barents–Kara Seas.

5. Abrupt shift of sea ice covariability pattern since the late 1990s

So far we have demonstrated that the early winter quadrupole pattern can be mostly attributed to the atmospheric wave-2 pattern, which may closely relate to the intense ice–atmosphere interaction processes in the Grn–BaK. However, it is unclear what causes the breakdown of the connection between the Grn–BaK SIE and the Ber SIE in the later period. Taking into account the fast equatorward expansion of BaK SIE in October–November and the notable shrinking of BaK SIE since 1998 (Fig. 2), we intuitively suppose that the interruption of the covariability of sea ice cover in the late period may be closely linked to the continuous retreat of the BaK SIE. In the BaK, the sea ice is relatively thin compared to the rest of the Arctic Ocean. The thin layer of ice is very sensitive to changes in both the atmosphere and ocean. In turn, the BaK sea ice change

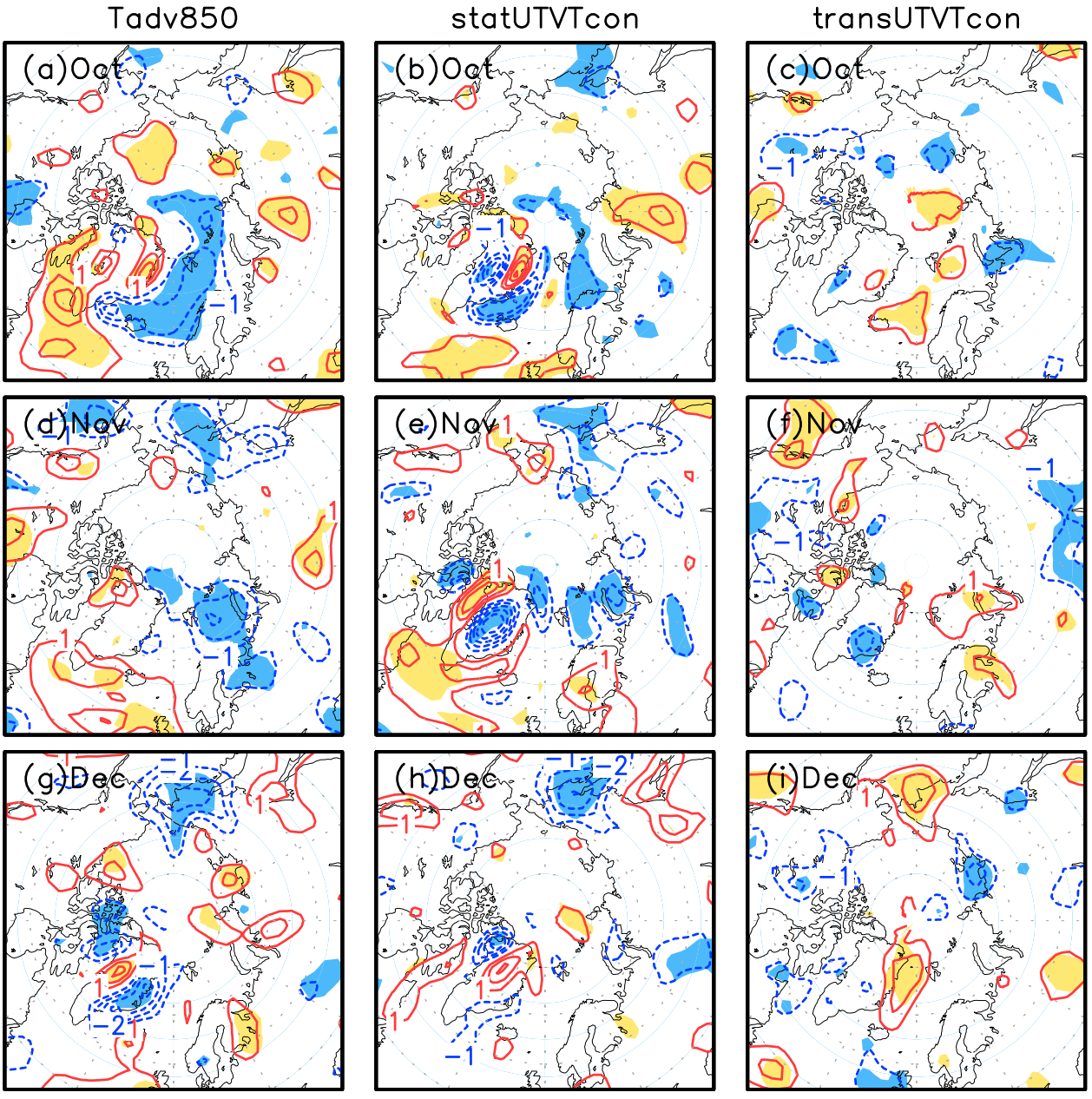

FIG. 11. (a) Detrended October 850-hPa temperature advection composites based on the November Greenland–Barents–Kara sea ice extent indices (high minus low events). Contour interval is 1 K day^{-1}, and the shaded areas denote the 95% significance level. (b) As in (a), but for 850-hPa stationary wave heat flux convergence. (c) As in (a), but for 850-hPa transient wave heat flux convergence. (d)–(f) As in (a)–(c), but for the month of November. (g)–(i) As in (a)–(c), but for the month of December.

can impact the atmospheric circulation change by adjusting the ocean–atmosphere turbulent heat flux and solar shortwave radiation. With large air–sea temperature difference in wintertime, the turbulent heat flux from an open ocean may reach 300–500 W m^{-2}, which is almost two orders of magnitude larger than through the ice (Andreas 1980; Simonsen and Haugan 1996). Here we present the monthly correlations between the BaK SIE and the total atmospheric heating rate (including the net shortwave radiation flux, the net longwave radiation flux, and the latent and sensible heat flux) over the BaK ice edge zone (BaKIEZ; referring to Fig. 1b) in Fig. 12a. The early winter BaK SIE negatively correlates with the atmospheric heating rate by sea ice leading about one month. It means that the retreat of BaK SIE favors both the enhanced heat flux from ocean and the

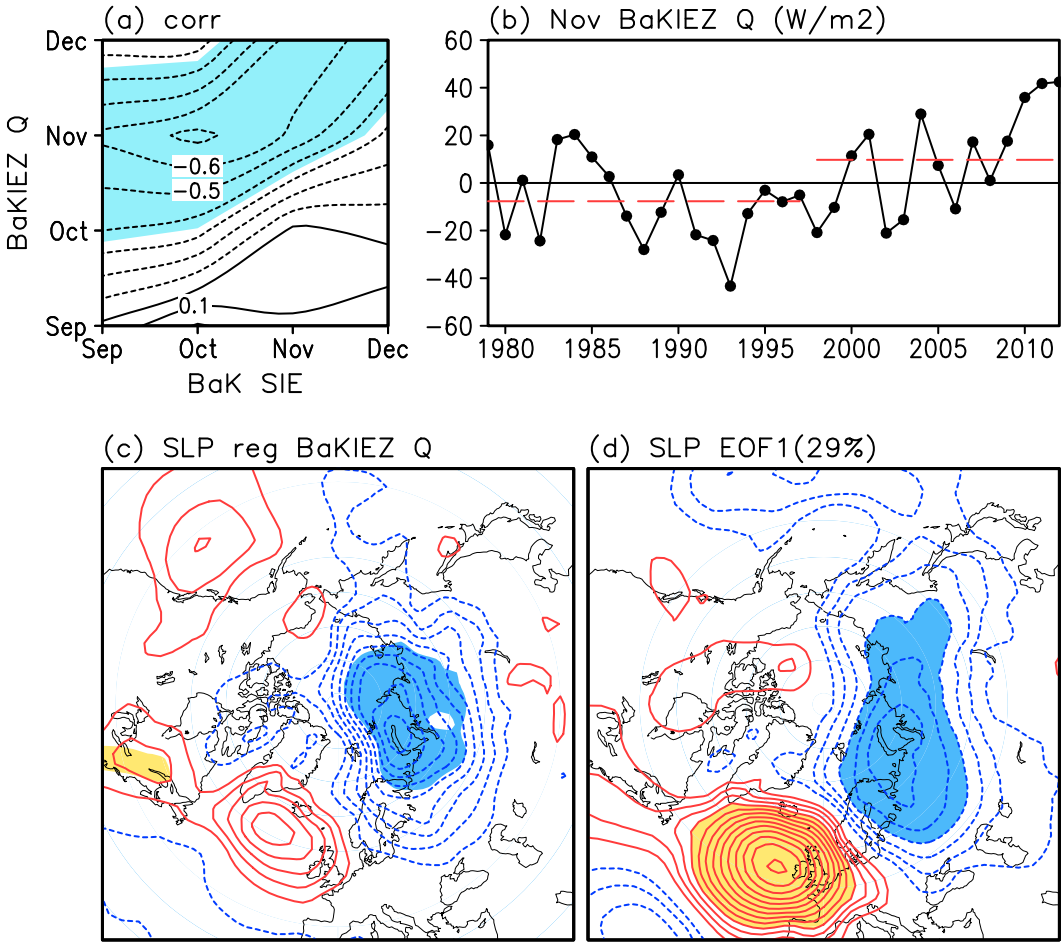

FIG. 12. (a) Detrended lead–lag correlations between the BaK SIE and the BaK ice edge zone heating rate during the period of 1979–2012. The contour interval is 0.1, and the shaded area denotes the correlation coefficients above the 95% significance level of Student's *t* test. (b) Time series of November BaK ice edge zone heating rate anomalies. The red dashed lines indicate the mean values for the early period (1979–97) and the late period (1998–2012). (c) Regression of 1998–2012 detrended November sea level pressure anomalies on the time series of November BaK ice edge zone heating rate anomalies. Contour intervals are 0.5 hPa, with the 95% significance level signified by the shaded area. (d) The leading EOF mode of sea level pressure in November during the period of 1998–2012. Contour intervals are 0.5 hPa, with the shaded area denoting SLP anomalies above (below) 2 hPa (−2 hPa).

reduced reflection of solar shortwave radiation, leading to the local heating of the atmosphere. Following the fast retreat of BaKIEZ, the November BaK ice edge zone heating rate exhibits the upward trend after 1998 (Fig. 12b). Particularly in the recent 3 yr, the anomalous heating rate even exceeds 40 W m^{-2}. The atmospheric circulation responds to the successive increase of heating rate in the lower boundary, displaying a significant low pressure anomaly over the BaK in the late period (Fig. 12c). Interestingly, the leading mode of November SLP EOF in the late period (Fig. 12d) also presents an anomalous low pressure over the BaK. In contrast to the early period (Fig. 7f), the SLP EOF1 anomalies over the Pacific sector are much weaker, and the zonal wave-2 pattern can be hardly identified in the late period. In addition, the regression of the original SLP (with trends included) onto the BaKIEZ heating rate presents a high consistency with the detrended regression pattern. This demonstrates the BaK sea ice retreat can really induce significant SLP anomalies and thus may contribute to the recent downward trend of SLP over the Barents–Kara Seas (figures not shown). The fact that the SLP leading mode and local SLP trends are both closely related to the BaK ice edge zone heating rate fully manifests the key roles of the BaK SIE in triggering the recent radical shift of atmospheric circulation.

According to our analysis in section 4, the early winter quadrupole pattern of sea ice resulted from the temperature advection and the stationary wave heat flux convergence associated with the atmospheric zonal

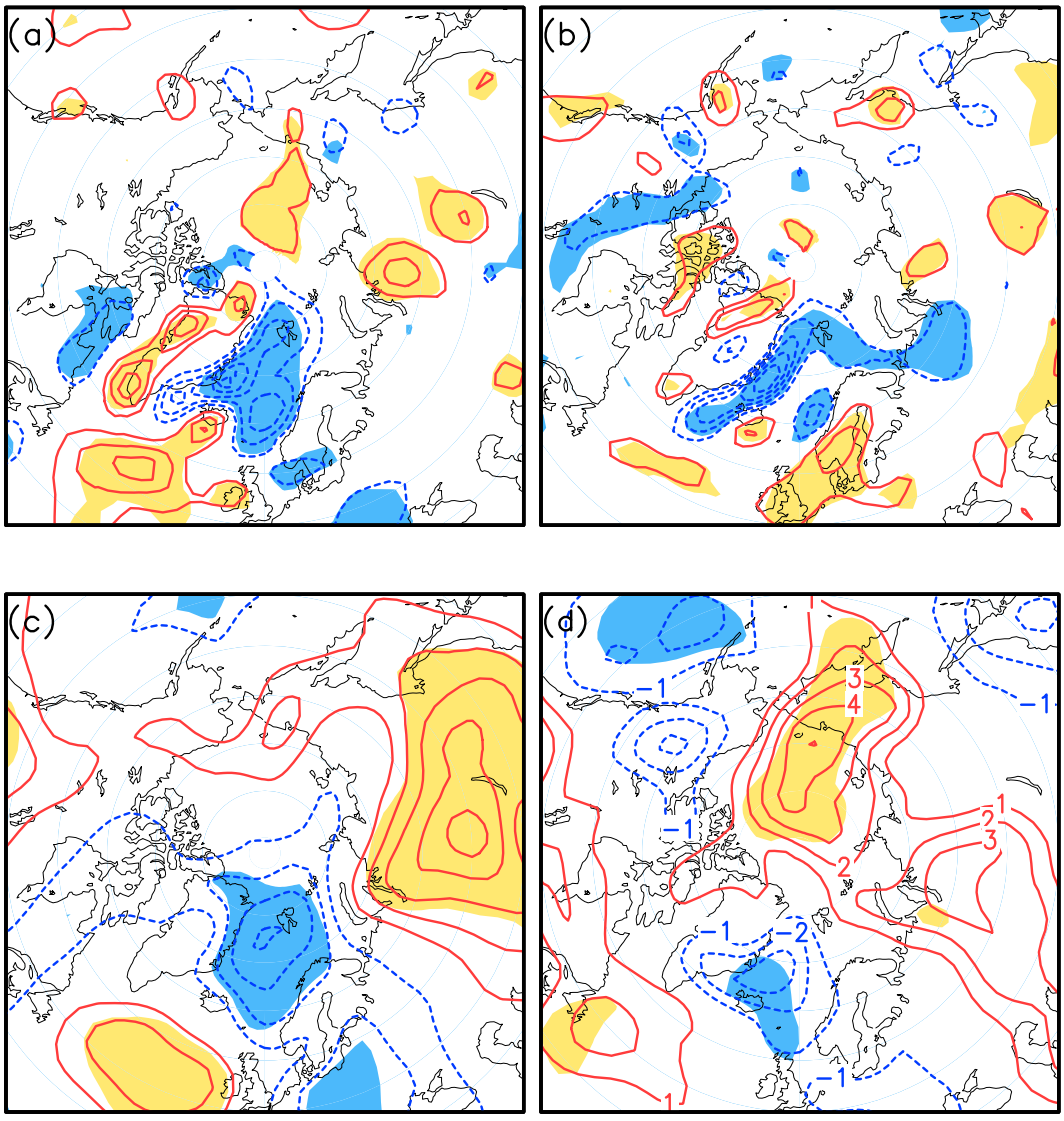

FIG. 13. (a) Regression of detrended November 850-hPa temperature advection anomalies on the time series of November SLP EOF1 during the period of 1998–2012. Contour intervals are 0.5 K day^{-1} with the 95% significance level signified by the shaded area. (b) As in (a), but for 850-hPa stationary wave heat flux convergence. (c) As in (a), but for 850-hPa air temperature. (d) Detrended November 850-hPa air temperature composites on the November GrnSIE−BaKSIE+ minus GrnSIE+BaKSIE− (see Table 1).

wave-2 pattern. To investigate the cause of breakdown of the early winter quadrupole pattern, the 850-hPa temperature advection, stationary wave heat flux convergence, and 850-hPa temperature anomalies are regressed on the principle component of November SLP EOF during the late period (Figs. 13a–c). Significant cold advection prevails over the Grn, in association with the northerly winds at the west flank of the low pressure anomaly in Fig. 12d. In the meantime, the anomalous stationary wave heat flux diverges over the same region. The cold advection and heat flux divergence together contribute to the cold air temperature anomalies. Figure 13d shows the composite analysis based on the late period out-of-phase variation of the Grn–BaK SIE (GrnSIE+BaKSIE− minus GrnSIE−BaKSIE+; see Table 1, columns 3 and 4). The cold anomalies over the Grn are mostly reproduced in the composites, denoting that Grn SIE variability in the late period is still under the spell of the overlying atmospheric circulation. On the contrary, there are no significant temperature advection and the heat flux convergence anomalies over the BaK. Thus, the 850-hPa air temperature over the BaK disconnects with the atmospheric circulation, and the local sea ice variability seems to be out of control of

the atmospheric circulation. Our study is consistent with most previous studies in asserting that the sea ice cover in the BaK is getting more sensitive to the ice–albedo feedback rather than to the atmospheric circulation variability in recent years. In addition, there are no significant air temperature anomalies over the Ber because of the weakening of wave-2 pattern, leading to the disconnection between the Grn–BaK SIE and the Ber SIE in the late period.

6. Conclusions and discussion

This study reveals a prominent discrepancy of sea ice variability between early winter and late winter. Although the double dipole patterns (one over the North Atlantic and the other over the North Pacific) are steadily established throughout the wintertime, the sea ice cover in the Grn–BaK varies in phase with that in the Ber in early winter (November and December). This early winter quadrupole pattern is different from the quadrupole pattern in late winter, in which the Grn–BaK SIC is out of phase with the Ber SIC. In addition, the in-phase variation during early winter follows an anticlockwise sequence, which shows that the Grn SIE leads the BaK SIE by 1 month and the Ber SIE by about 2 months. The composite analyses illustrate that the planetary wave-2 pattern of atmospheric circulation plays a crucial role in driving this early winter sea ice pattern. The stationary wave first appears over the Atlantic section and then propagates its energy eastward and northward downstream, enhancing the zonal wave-2 pattern in November. The associated stationary wave heat flux divergence and cold temperature advection together cause the decreasing air temperature and the in-phase advance of sea ice cover in the Grn–BaK and the Ber. In the late period, however, the fast retreat of BaK SIE increases the local atmospheric heating rate, causing the formation of low pressure anomaly over the BaK. As a result, the atmospheric zonal wave-2 pattern collapses, and the connection between the Atlantic sector and Pacific sector is interrupted.

A consensus of previous studies is that the wintertime Arctic atmospheric circulation is dominated by the AO/NAO mode (EOF1) and the secondary Arctic dipole mode (EOF2) (Thompson et al. 2000; Wu et al. 2006). These two modes are both related to the sea ice variability and trends (Rigor and Wallace 2004; Steele et al. 2004; Wang et al. 2009). The stationary wave pattern, on the other hand, is also the ubiquitous characteristic in boreal winter. The winter planetary wave pattern is demonstrated to stimulate the atmospheric AL–IL seesaw pattern (Honda et al. 2001, 2005a) and influence the Arctic sea ice export through Fram Strait (Cavalieri 2002) and the Arctic Ocean circulation as a whole (Cavalieri and Häkkinen 2001). In addition, the early winter sea ice has been shown to impact the following middle and late winter climate through the stationary wave propagation over East Asia (Honda et al. 2009) and over the Pacific (Jaiser et al. 2012). Cohen et al. (2009) revealed that the Northern Hemisphere extratropical temperature trends appear asymmetric between early winter and late winter in the recent period, with vigorous warming in October–December followed by a reversal to a neutral/cold trend in January–March. They suggested this asymmetry is closely linked to the planetary wave activity, which in turn is forced by the anomalous Eurasian snow cover in the fall. In this study, we identify that the leading modes of atmospheric circulation are Arctic dipole mode in October and the zonal wave-2 pattern in November (Fig. 7), in contrast to the AO/NAO mode in late winter. We further discover that the stationary wave-2 pattern is strongly coupled to the Grn–BaK sea ice variability in November, which is critical to the early winter sea ice quadrupole pattern.

We recognize that many problems remain unresolved involving the recent climate regime shift. First, what is the main mechanism driving the fast Arctic sea ice reduction? The study by Deser and Teng (2008) revealed that the atmospheric forcing cannot account for the overall sea ice trends in both winter and summer, particularly for the continuous sea ice decline in the BaK since the 1990s. Our study suggests that this BaK sea ice decline in the 1990s is strongly connected to the summer sea ice albedo feedback and open water formation efficiency (Holland et al. 2006). In turn, the BaK sea ice retreat may feedback to the atmosphere thermodynamically because of the increasing amount of turbulent surface heat flux from the open water (Simonsen and Haugan 1996) and trigger the overall wintertime climate shift. In fact, some recent studies provided evidence of BaK sea ice in inducing the atmospheric baroclinic response, changing the Atlantic cyclone track, and impacting the AO polarity and the East Asian climate (Alexander et al. 2004; Deser et al. 2004; Inoue et al. 2012). Therefore, the sea ice–atmosphere interaction mechanism in this region deserves more detailed investigation for future research.

Another important issue is how long this climate regime will persist. The Arctic sea ice cover, along with the Arctic oceanic and atmospheric circulation, has long been viewed as varying on a decadal or multidecadal time scale (Mysak and Venegas 1998; Goosse et al. 2002; Goosse and Holland 2005). In the wake of the fast changing sea ice and atmospheric patterns in recent

years, the debate arises on whether Arctic sea ice has passed through a threshold, where after the Arctic climate is more controlled by sea ice albedo feedback and the summer Arctic Ocean is deemed to be sea ice free in the near future (Eisenman and Wettlaufer 2009; Wang and Overland 2012). Climate models simulated that the abrupt and irreversible sea ice retreat is caused by the increasing ocean heat transport (Holland et al. 2006), while other studies proposed recovery mechanisms that counteract the destabilizing ice–albedo effect after abrupt sea ice losses (Schröder and Connolley 2007; Tietsche et al. 2011). Our analysis here emphasizes that the wintertime sea ice pattern in the interannual time scale breaks down under the background of recent Arctic climate change, which is due largely to the decoupling of the sea ice cover and the atmosphere and to the weakening of the early winter stationary wave. Whether this is reversible may depend on future summer sea ice trends.

Acknowledgments. This research is supported by Office of Naval Research through Grant N00014-12-1-0911 and by the Natural Science Foundation of China (Grant 41006113), the Fundamental Research Funds for the Central Universities, and the Chinese Scholarship Fund. The authors thank Mingfang Ting for her helpful discussions.

REFERENCES

Alexander, M. A., U. S. Bhatt, J. E. Walsh, M. S. Timlin, J. S. Miller, and J. D. Scott, 2004: The atmospheric response to realistic Arctic sea ice anomalies in an AGCM during winter. *J. Climate,* **17,** 890–905, doi:10.1175/1520-0442(2004)017<0890:TARTRA>2.0.CO;2.

Alexeev, V. A., I. Esau, I. V. Polyakov, S. J. Byam, and S. Sorokina, 2012: Vertical structure of recent Arctic warming from observed data and reanalysis products. *Climatic Change,* **111,** 215–239, doi:10.1007/s10584-011-0192-8.

Andreas, E. L, 1980: Estimation of heat and mass fluxes over Arctic leads. *Mon. Wea. Rev.,* **108,** 2057–2063, doi:10.1175/1520-0493(1980)108<2057:EOHAMF>2.0.CO;2.

Blanchard-Wrigglesworth, E., K. C. Armour, C. M. Bitz, and E. DeWeaver, 2011: Persistence and inherent predictability of Arctic sea ice in a GMC ensemble and observations. *J. Climate,* **24,** 231–250, doi:10.1175/2010JCLI3775.1.

Cavalieri, D. J., 2002: A link between Fram Strait sea ice export and atmospheric planetary wave phase. *Geophys. Res. Lett.,* **29,** 1614, doi:10.1029/2002GL014684.

——, and S. Häkkinen, 2001: Arctic climate and atmospheric planetary waves. *Geophys. Res. Lett.,* **28,** 791–794, doi:10.1029/2000GL011855.

——, C. L. Parkinson, P. Gloersen, and H. J. Zwally, cited 2013: Sea ice concentrations from Nimbus-7 SMMR and DMSP SSM/I-SSMIS passive microwave data. National Snow and Ice Data Center. [Available online at http://nsidc.org/data/nsidc-0051.html.]

Chapman, W. L., and J. E. Walsh, 2007: Simulations of Arctic temperature and pressure by global coupled models. *J. Climate,* **20,** 609–632, doi:10.1175/JCLI4026.1.

Cohen, J., and M. Barlow, 2005: The NAO, the AO, the global warming: How closely related? *J. Climate,* **18,** 4498–4513, doi:10.1175/JCLI3530.1.

——, ——, and K. Saito, 2009: Decadal fluctuations in planetary wave forcing modulate global warming in late boreal winter. *J. Climate,* **22,** 4418–4426, doi:10.1175/2009JCLI2931.1.

Comiso, J. C., C. L. Parkinson, R. Gersten, and L. Stock, 2008: Accelerated decline in the Arctic sea ice cover. *Geophys. Res. Lett.,* **35,** L01703, doi:10.1029/2007GL031972.

Deser, C., and H. Teng, 2008: Evolution of Arctic sea ice concentration trends and the role of atmospheric circulation forcing, 1979–2007. *Geophys. Res. Lett.,* **35,** L02504, doi:10.1029/2007GL032023.

——, J. E. Walsh, and M. S. Timlin, 2000: Arctic sea ice variability in the context of recent atmospheric circulation trends. *J. Climate,* **13,** 617–633, doi:10.1175/1520-0442(2000)013<0617:ASIVIT>2.0.CO;2.

——, G. Magnusdottir, R. Saravanan, and A. Phillips, 2004: The effects of North Atlantic SST and sea ice anomalies on the winter circulation in CCM3. Part II: Direct and indirect components of the response. *J. Climate,* **17,** 877–889, doi:10.1175/1520-0442(2004)017<0877:TEONAS>2.0.CO;2.

——, R. Tomas, M. Alexander, and D. Laurence, 2010: The seasonal atmospheric response to projected Arctic sea ice loss in the late twenty-first century. *J. Climate,* **23,** 333–351, doi:10.1175/2009JCLI3053.1.

Eisenman, I., and J. S. Wettlaufer, 2009: Nonlinear threshold behavior during the loss of Arctic sea ice. *Proc. Natl. Acad. Sci. USA,* **106,** 28–32, doi:10.1073/pnas.0806887106.

Fang, Z., and J. M. Wallace, 1994: Arctic sea ice variability on a timescale of weeks and its relation to atmospheric forcing. *J. Climate,* **7,** 1897–1914, doi:10.1175/1520-0442(1994)007<1897:ASIVOA>2.0.CO;2.

Francis, J. A., and E. Hunter, 2007: Drivers of declining sea ice in the Arctic winter: A tale of two seas. *Geophys. Res. Lett.,* **34,** L17503, doi:10.1029/2007GL030995.

——, W. Chan, D. J. Leathers, J. R. Miller, and D. E. Veron, 2009: Winter Norther Hemisphere weather patterns remember summer Arctic sea-ice extent. *Geophys. Res. Lett.,* **36,** L07503, doi:10.1029/2009GL037274.

Goosse, H., and M. M. Holland, 2005: Mechanisms of decadal Arctic climate variability in the Community Climate System Model, version 2 (CCSM2). *J. Climate,* **18,** 3552–3570, doi:10.1175/JCLI3476.1.

——, F. M. Selten, R. J. Haarsma, and J. D. Opsteegh, 2002: A mechanism of decadal variability of the sea-ice volume in the Northern Hemisphere. *Climate Dyn.,* **19,** 61–83, doi:10.1007/s00382-001-0209-5.

Holland, M. M., 2013: The great sea-ice dwindle. *Nat. Geosci.,* **6,** 10–11, doi:10.1038/ngeo1681.

——, C. M. Bitz, and B. Tremblay, 2006: Future abrupt reductions in the summer Arctic sea ice. *Geophys. Res. Lett.,* **33,** L23503, doi:10.1029/2006GL028024.

Honda, M., H. Nakamura, J. Ukita, I. Kousaka, and K. Takeuchi, 2001: Interannual seesaw between the Aleutian and Icelandic lows. Part I: Seasonal dependence and life cycle. *J. Climate,* **14,** 1029–1042, doi:10.1175/1520-0442(2001)014<1029:ISBTAA>2.0.CO;2.

——, Y. Kushnir, H. Nakamura, S. Yamane, and S. E. Zebiak, 2005a: Formation, mechanisms, and predictability of the

Aleutian–Icelandic low seesaw in ensemble AGCM simulations. *J. Climate,* **18,** 1423–1434, doi:10.1175/JCLI3353.1.

——, S. Yamane, and H. Nakamura, 2005b: Impacts of the Aleutian–Icelandic low seesaw on surface climate during the twentieth century. *J. Climate,* **18,** 2793–2802, doi:10.1175/JCLI3419.1.

——, J. Inoue, and S. Yamane, 2009: Influence of low Arctic sea-ice minima on anomalous cold Eurasian winters. *Geophys. Res. Lett.,* **36,** L08707, doi:10.1029/2008GL037079.

Hopsch, S., J. Cohen, and K. Dethloff, 2012: Analysis of a link between fall Arctic sea ice concentration and atmospheric patterns in the following winter. *Tellus,* **64A,** 18624, doi:10.3402/tellusa.v64i0.18624.

Inoue, J., M. E. Hori, and K. Takaya, 2012: The role of Barents Sea ice in the wintertime cyclone track and emergence of a warm-Arctic cold-Siberian anomaly. *J. Climate,* **25,** 2561–2568, doi:10.1175/JCLI-D-11-00449.1.

Jaiser, R., K. Dethloff, D. Handorf, A. Rinke, and J. Cohen, 2012: Impact of sea ice cover changes on the Northern Hemisphere atmospheric winter circulation. *Tellus,* **64A,** 11595, doi:10.3402/tellusa.v64i0.11595.

Kalnay, E., and Coauthors, 1996: The NCEP/NCAR 40-Year Reanalysis Project. *Bull. Amer. Meteor. Soc.,* **77,** 437–471, doi:10.1175/1520-0477(1996)077<0437:TNYRP>2.0.CO;2.

Lindsay, R. W., and J. Zhang, 2005: The thinning of Arctic sea ice, 1988–2003: Have we passed a tipping point? *J. Climate,* **18,** 4879–4894, doi:10.1175/JCLI3587.1.

Maslanik, J. A., C. Fowler, J. Stroeve, S. Drobot, J. Zwally, D. Yi, and W. Emery, 2007: A younger, thinner Arctic ice cover: Increased potential for rapid, extensive sea-ice loss. *Geophys. Res. Lett.,* **34,** L24501, doi:10.1029/2007GL032043.

Mysak, L. A., and S. A. Venegas, 1998: Decadal climate oscillations in the Arctic: A new feedback loop for atmosphere-ice-ocean interactions. *Geophys. Res. Lett.,* **25,** 3607–3610, doi:10.1029/98GL02782.

Nghiem, S. V., I. G. Rigor, D. K. Perovich, P. Clemente-Colón, J. W. Weatherly, and G. Neumann, 2007: Rapid reduction of Arctic perennial sea ice. *Geophys. Res. Lett.,* **34,** L19504, doi:10.1029/2007GL031138.

Orsolini, Y. J., R. Senan, R. E. Benestad, and A. Melsom, 2012: Autumn atmospheric response to the 2007 low Arctic sea ice extent in coupled ocean–atmosphere hindcasts. *Climate Dyn.,* **38,** 2437–2448, doi:10.1007/s00382-011-1169-z.

Overland, J. E., and M. Wang, 2005: The Arctic climate paradox: The recent decrease of the Arctic Oscillation. *Geophys. Res. Lett.,* **32,** L06701, doi:10.1029/2004GL021752.

——, ——, and S. Salo, 2008: The recent Arctic warm period. *Tellus,* **60A,** 589–597, doi:10.1111/j.1600-0870.2008.00327.x.

Parkinson, C. L., and D. J. Cavalieri, 2008: Arctic sea ice variability and trends, 1979-2006. *J. Geophys. Res.,* **113,** C07003, doi:10.1029/2007JC004558.

——, and J. C. Comiso, 2013: On the 2012 record low Arctic sea ice cover: Combined impact of preconditioning and an August storm. *Geophys. Res. Lett.,* **40,** 1356–1361, doi:10.1002/grl.50349.

Plumb, R. A., 1985: On the three-dimensional propagation of stationary waves. *J. Atmos. Sci.,* **42,** 217–229, doi:10.1175/1520-0469(1985)042<0217:OTTDPO>2.0.CO;2.

Polyakov, I. V., A. V. Pnyushkov, and L. A. Timokhov, 2012: Warming of the intermediate Atlantic water of the Arctic Ocean in the 2000s. *J. Climate,* **25,** 8362–8370, doi:10.1175/JCLI-D-12-00266.1.

Proshutinsky, A. Y., and M. A. Johnson, 1997: Two circulation regimes of the wind-driven Arctic Ocean. *J. Geophys. Res.,* **102,** 12 493–12 514, doi:10.1029/97JC00738.

Rayner, N. A., D. E. Parker, E. B. Horton, C. K. Folland, L. V. Alexander, D. P. Rowell, E. C. Kent, and A. Kaplan, 2003: Global analyses of sea surface temperature, sea ice, and night marine air temperature since the late nineteenth century. *J. Geophys. Res.,* **108,** 4407, doi:10.1029/2002JD002670.

Rigor, I. G., and J. M. Wallace, 2004: Variations in the age of Arctic sea-ice and summer sea-ice extent. *Geophys. Res. Lett.,* **31,** L09401, doi:10.1029/2004GL019492.

——, ——, and R. L. Colony, 2002: Response of sea ice to the Arctic Oscillation. *J. Climate,* **15,** 2648–2663, doi:10.1175/1520-0442(2002)015<2648:ROSITT>2.0.CO;2.

Rogers, J. C., and M.-P. Hung, 2008: The Odden ice feature of the Greenland Sea and its association with atmospheric pressure, wind, and surface flux variability from reanalyses. *Geophys. Res. Lett.,* **35,** L08504, doi:10.1029/2007GL032938.

Schröder, D., and W. M. Connolley, 2007: Impact of instantaneous sea ice removal in a coupled general circulation model. *Geophys. Res. Lett.,* **34,** L14502, doi:10.1029/2007GL030253.

Screen, J. A., and I. Simmonds, 2010: The central role of diminishing sea ice in recent Arctic temperature amplification. *Nature,* **464,** 1334–1337, doi:10.1038/nature09051.

——, ——, C. Deser, and R. Tomas, 2013: The atmospheric response to three decades of observed Arctic sea ice loss. *J. Climate,* **26,** 1230–1248, doi:10.1175/JCLI-D-12-00063.1.

Serreze, M. C., and R. G. Barry, 2011: Processes and impacts of Arctic amplification: A research synthesis. *Global Planet. Change,* **77,** 85–96, doi:10.1016/j.gloplacha.2011.03.004.

——, M. M. Holland, and J. Stroeve, 2007: Perspectives on the Arctic's shrinking sea-ice cover. *Science,* **315,** 1533–1536, doi:10.1126/science.1139426.

Shuchman, R. A., E. G. Josberger, C. A. Russel, K. W. Fischer, O. M. Johannessen, J. Johannessen, and P. Gloersen, 1998: Greenland Sea Odden sea ice feature: Intra-annual and interannual variability. *J. Geophys. Res.,* **103,** 12 709–12 724, doi:10.1029/98JC00375.

Simonsen, K., and P. M. Haugan, 1996: Heat budgets of the Arctic Mediterranean and sea surface heat flux parameterizations for the Nordic Seas. *J. Geophys. Res.,* **101,** 6553–6576, doi:10.1029/95JC03305.

Steele, M., J. Morison, W. Ermold, I. Rigor, M. Ortmeyer, and K. Shimada, 2004: Circulation of summer Pacific halocline water in the Arctic Ocean. *J. Geophys. Res.,* **109,** C02027, doi:10.1029/2003JC002009.

Strey, S. T., W. L. Chapman, and J. E. Walsh, 2010: The 2007 sea ice minimum: Impacts on the Northern Hemisphere atmosphere in late autumn and early winter. *J. Geophys. Res.,* **115,** D23103, doi:10.1029/2009JD013294.

Stroeve, J., M. M. Holland, W. Meier, T. Scambos, and M. Serreze, 2007: Arctic sea ice decline: Faster than forecast. *Geophys. Res. Lett.,* **34,** L09501, doi:10.1029/2007GL029703.

——, M. C. Serreze, M. M. Holland, J. E. Kay, J. Malanik, and A. P. Barrett, 2012: The Arctic's rapidly shrinking sea ice cover: A research synthesis. *Climatic Change,* **110,** 1005–1027, doi:10.1007/s10584-011-0101-1.

Thompson, D. W. J., J. M. Wallace, and G. C. Hegerl, 2000: Annular modes in the extratropical circulation. Part II: Trends. *J. Climate,* **13,** 1018–1036, doi:10.1175/1520-0442(2000)013<1018:AMITEC>2.0.CO;2.

Tietsche, S., D. Notz, J. H. Jungclaus, and J. Marotzke, 2011: Recovery mechanisms of Arctic summer sea ice. *Geophys. Res. Lett.,* **38,** L02707, doi:10.1029/2010GL045698.

Wang, J., J. Zhang, E. Watanabe, M. Ikeda, K. Mizobata, J. E. Walsh, X. Bai, and B. Wu, 2009: Is the dipole anomaly a major driver to record lows in Arctic summer sea ice extent? *Geophys. Res. Lett.,* **36,** L05706, doi:10.1029/2008GL036706.

Wang, M., and J. E. Overland, 2012: A sea ice free summer Arctic within 30 years: An update from CMIP5 models. *Geophys. Res. Lett.,* **39,** L18501, doi:10.1029/2012GL052868.

Wu, B., J. Wang, and J. E. Walsh, 2006: Dipole anomaly in the winter Arctic atmosphere and its association with sea ice motion. *J. Climate,* **19,** 210–225, doi:10.1175/JCLI3619.1.

Yang, X.-Y., J. C. Fyfe, and G. M. Flato, 2010: The role of poleward energy transport in Arctic temperature evolution. *Geophys. Res. Lett.,* **37,** L14803, doi:10.1029/2010GL043934.

Zhang, X., M. Ikeda, and J. E. Walsh, 2003: Arctic sea ice and freshwater changes driven by the atmospheric leading mode in a coupled sea ice–ocean model. *J. Climate,* **16,** 2159–2177, doi:10.1175/2758.1.

——, A. Sorteberg, J. Zhang, R. Gerdes, and J. C. Comiso, 2008: Recent radical shifts of atmospheric circulations and rapid changes in Arctic climate system. *Geophys. Res. Lett.,* **35,** L22701, doi:10.1029/2008GL035607.